Artificial Neural Network-Based MPPT Controller for PV System Integrated with Grid and Induction Motor

Priyanka Nikhil Mane, Rushikesh Sunil Suryawanshi, Neel Ajit Mangave,
Harshal Anandrao Nalawade and Ayan Firoj Sayyad
Department of Electrical Engineering, Kolhapur Institute of Technology's College of Engineering (Empowered Autonomous), Kolhapur, India

Keywords: PV, ANN Based MPPT, VSI, PI, LC Filter, SVPWM.

Abstract: The integration of a Photovoltaic (PV) system with an induction motor and grid offers a sustainable solution for energy generation and utilization, particularly in industrial and commercial applications. However, to guarantee effective functioning, it is essential to optimize the power extracted from PV system. The PV system's operating point, which fluctuates with external conditions including temperature and sun irradiation, must be dynamically adjusted by a Maximum Power Point Tracking (MPPT) controller in order to capture maximum amount of power. Traditional MPPT algorithms, while effective, may not always provide optimal performance in fluctuating conditions. To address this, an Artificial Neural Network (ANN) based MPPT controller enhance the tracking accuracy and efficiency. By learning from system behavior and adjusting in real-time, the ANN-based controller outperforms conventional methods, offering superior performance and faster convergence to Maximum Power Point (MPP). When integrated with the grid and an induction motor, this intelligent MPPT controller ensures not only optimal energy extraction from the PV system but also stable power delivery. The induction motor, driven by solar energy, operates efficiently with minimal energy losses, while the grid connection facilitates the exchange of power, ensuring system stability. Simulation results are obtained using MATLAB, showing that efficiency of the tracking method is 93.5% and the THD value of 2%.

1 INTRODUCTION

In recent years, induction motors have become indispensable in various industries, serving as the backbone for many essential operations. Induction motors account for over 40% of global electric power consumption, reflecting their widespread usage. These motors are used to drive machinery in sectors such as manufacturing, water pumping, HVAC systems, and various types of compressors. Their widespread application is primarily due to their versatility, durability, and cost-effectiveness, making them the preferred choice for industrial operations that require reliable, continuous power. However, as society progresses and the demand for electric motors continues to rise, so does the need for more electrical energy. This surge in demand has put significant pressure on existing power generation systems, exacerbating the strain on traditional energy sources.

Fossil fuels, the primary source of energy in many parts of world, are becoming less sustainable due to the increasing environmental concerns they generate. The emission of greenhouse gases and depletion of non-renewable resources have led to mounting restrictions on expanding fossil fuel-based energy sources.

To combat these issues and meet growing demand for energy, Renewable Energy Systems (RES), especially solar power, are being increasingly embraced. Solar energy, captured through PV systems, offers a clean, sustainable and abundant energy source. The integration of RES with technologies such as induction motors presents an opportunity for industries to operate in a more energy-efficient and environmentally friendly manner. By utilizing solar energy to power induction motors, industries reduce their reliance on conventional, polluting energy sources and decrease their carbon footprint. This integration not only addresses the global energy demand but also promotes a greener, more sustainable future by mitigating the environmental impacts of traditional

Mane, P. N., Suryawanshi, R. S., Mangave, N. A., Nalawade, H. A. and Sayyad, A. F.
Artificial Neural Network-Based MPPT Controller for PV System Integrated with Grid and Induction Motor.
DOI: 10.5220/0013642900004664

In *Proceedings of the 3rd International Conference on Futuristic Technology (INCOFT 2025) - Volume 3*, pages 721-732
ISBN: 978-989-758-763-4

energy production. The voltage from the PV system is increased using a boost converter.

Tracking mechanisms such as Hill Climbing (Moll and Linda, 2023 – Glowed and Masoud, 2020), Incremental Conductance (IncCond) (Karan, Bashar, et al. 2022), and Perturb and Observe (P&O) (Mohammad, 2024) play a vital role in accurately measuring the power extracted from PV systems. Among these, P&O method is known for its high accuracy and adaptability, however it is sensitive to variations in solar irradiance, temperature, and panel orientation. IncCond enhances efficiency and reduces oscillations, providing more stable tracking nevertheless it faces challenges in terms of space, weight, and maintenance. Hill Climbing offers reliable tracking and flexibility in system configurations, however it requires significant computational resources. To address these limitations, this work proposes the implementation of an ANN-based MPPT technique, which improves energy efficiency, ensures precise tracking of the optimal power from PV systems, and offers exceptional adaptability for a range of solar power applications. The key contributions of this study are:

- To maximise the utilisation of renewable energy sources and preserve grid stability, PV systems must be integrated with the electrical grid and BLDC motor.
- The implementation of Boost converter boosts the low PV panel voltage, improves efficiency and enhances the reliability of the PV system.
- ANN based MPPT method is implemented to track maximum power generated by PV system.

2 PROPOSED SYSTEM DESCRIPTION

In this work, a PV system is designed for efficient energy conversion and seamless integration with the grid, utilizing advanced control techniques for optimal performance. When sunlight is converted into Direct Current (DC) electrical energy by solar panels, a boost converter increases voltage to appropriate level for further processing. Using an MPPT algorithm, which continuously modifies PV array's operating point to collect maximum power under changing environmental conditions, energy extraction is maximized. The increased voltage is fed into a Pulse-Width Modulation (PWM) generator, which generates PWM pulses to regulate a converter's switching function. The power is delivered to an induction motor, with a proportional-integral (PI) controller managing the power flow and optimizing energy delivery while adapting to varying load conditions. For accurate VSI control, the system additionally uses Space Vector Pulse Width Modulation (SVPWM), which guarantees ideal voltage regulation and effective inverter operation. Additionally, a three-phase voltage source inverter (VSI) is used to send excess power from PV system to the grid. This ensures a stable and effective interaction between PV system and the grid by controlling the power transfer. Figure 1 displays the proposed work's block diagram.

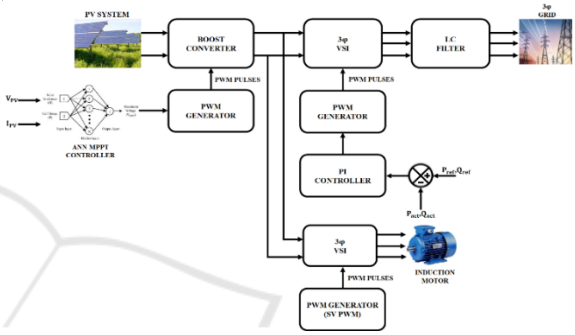

Figure 1: Proposed Block Diagram

3 SYSTEM MODELLING

3.1 PV System

The core part of a solar energy system, a PV cell converts sunlight directly into electrical energy. The electrical properties of a large diode is seen in a PV cell.

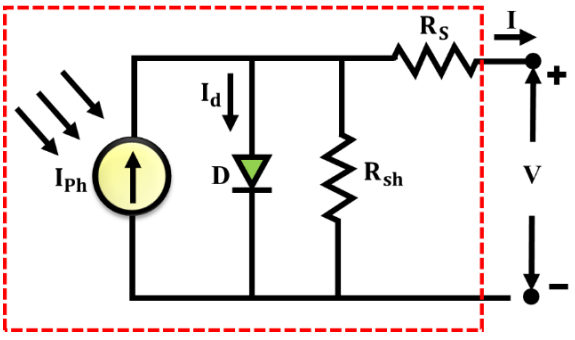

Figure 2: PV cell

When exposed to light, the output current is the sum of the dark current (I_d) and the photocurrent (I_{ph}), which is expressed as:

$$I = I_{ph} - I_d \quad (1)$$

The equivalent circuit of PV system is shown in Figure 2. In practical, A series resistance is used to dissipate electricity (R_s) caused by ohmic contact on the front surface, and a shunt resistance (Rsh) due to leakage current, as depicted in Figure 2. Therefore, the Equation 1 is written as:

$$I = I_{ph} - I_d - I_{sh} \quad (2)$$

A PV system's output voltage, which is typically low, is increased with a boost converter.

3.2 Boost Converter

A number of important parts are arranged in a specific way in the boost converter's schematic diagram, which is displayed in Figure 3. Notably, circuit features parallel-connected inductors and switches, with the inductor (L) and switch (S) also arranged in parallel. Additionally, the diode (D) is configured in parallel, creating two parallel paths between the input and output circuits. This configuration improves the converter's performance and reliability, making it ideal for a range of power conversion applications.

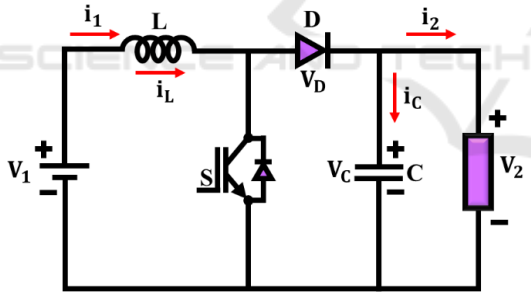

Figure 3: Equivalent circuit of Boost converter

Mode 1: In mode 1, switch S is in ON condition and diode D is in OFF condition, where the inductor L is charging and the capacitor C is discharging.

Mode 2: In mode 2, Diode D is in ON condition, and switch S is in OFF condition, where Capacitor C is charging and Inductor L is discharging.

Figure 5 represents the switching waveform of the boost converter. Boost converters often exhibit nonlinear dynamics due to switching operations, control loops, and varying loads. The ANN-based MPPT controller is well-suited to model these nonlinearities, providing a more accurate representation of the converter's behavior. Additionally, the tracking of the converter's output is achieved using an ANN-based MPPT controller.

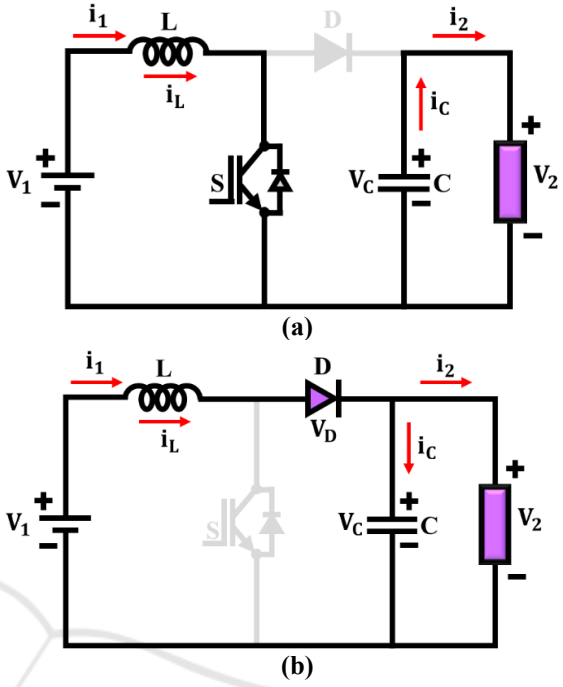

Figure 4: Equivalent Circuit of Boost converter (a) Mode 1, (b) Mode 2

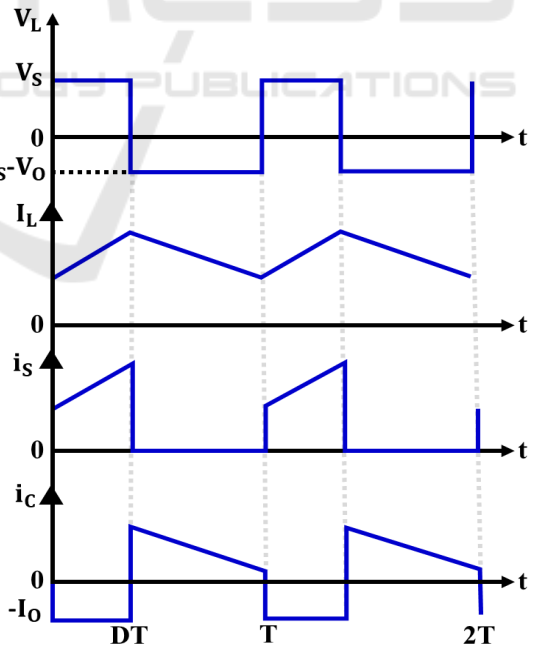

Figure 5: Switching Waveform

3.3 ANN based MPPT Algorithm

The ANN based MPPT algorithm uses ANN to optimize the MPPT of PV systems. By learning relationship between environmental factors and the system's output power, ANN predict and adjust the operating point to ensure maximum power extraction.

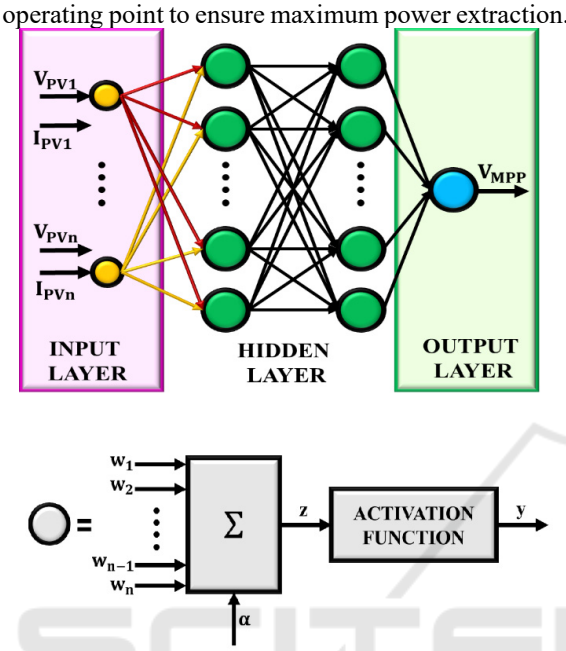

Figure 6: Architecture of ANN based MPPT

$$Mapminmax = \frac{(x-x_{min})(x_{max}-x_{min})}{(y_{max}-y_{min})} + y_{min} \quad (3)$$

$$Tansig = \frac{2}{e^{-2x}+1} - 1 \quad (4)$$

$$Mapminmax\_rever = \frac{(x-y_{min})(x_{max}-x_{min})}{(y_{max}-y_{min})} + x_{min} \quad (5)$$

As shown in Equation 3, $Mapminmax$ function is employed to normalize input values. In the hidden layer, the $Tansig$ function, as defined in Equation 4, serves as the activation function. The normalized values are then reverted to their original values using the $Mapminmax\_rever$ function, as indicated in Equation 5.

$$y_j = f(\sum w_{ij} x_i + b) \quad (6)$$

Where x_i is the input signal, w_{ij} represents the connection weight, f is the activation function, y_j is the output neuron and b is the bias value.

$$E = \frac{1}{2}\sum_j (y_{dj} - y_j)^2 \quad (7)$$

The performance of ANN is evaluated using regression coefficient R^2. These performance metrics are defined in Equations 8 and 9, respectively.

$$MSE = \frac{\sum_{i=1}^{n}(y_{p,i}-y_i)^2}{n} \quad (8)$$

$$R^2 = 1 - \frac{\sum_{i=1}^{n}(y_{p,i}-y_i)^2}{\sum_{i=1}^{n}(y_{m,1})^2} \quad (9)$$

Where $y_{p,i}$ is the estimated value, n is the sample size,$y_{m,1}$is the measured value, and y_i is the value of the sampled data.

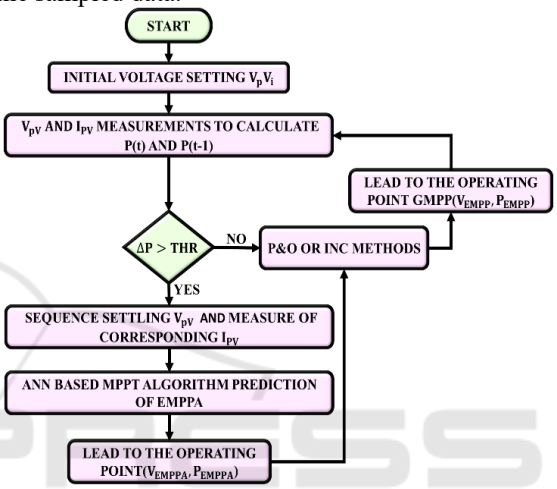

Figure 7: Flowchart of ANN based MPPT

Flowchart of ANN based MPPT algorithm is represented in Figure 7, which enhances tracking efficiency, reduces computation time, and improves overall system performance.

3.4 Induction Motor

A active electric motor type in industrial settings is the induction motor, which is dependable, long-lasting, and requires low maintenance. It spins by creating a revolving magnetic field that causes the rotor to conduct current. Particularly when combined with RES, it is essential to many energy-efficient systems. The speed of the induction motor is expressed as:

$$V_{ds}^s = i_{ds}^s R_s + L_{ls}\frac{d}{dt}(i_{ds}^s) + \frac{d}{dt}(\psi_{dm}^s) \quad (10)$$

$$V_{ds}^s = \frac{L_m}{L_r}\frac{d}{dt}(\psi_{dr}^s) + R_s \sigma L_s) i_{ds}^s \quad (11)$$

Where, $\sigma = 1 - \frac{L_m^2}{L_r L_s}$

Similarly,

$$\frac{d}{dt}(\psi_{qr}^s) = \frac{L_r}{L_m} v_{qs}^s - \frac{L_r}{L_m}(R_s + \sigma L_s S) i_{qs}^s \quad (12)$$

$$\frac{d}{dt}(\psi_{dr}^{s}) = \frac{L_m}{T_r} i_{ds}^{s} - \omega_r \psi_{qr}^{s} - \frac{1}{T_r}\psi_{dr}^{s} \quad (13)$$

$$\frac{d}{dt}(\psi_{dr}^{s}) = \frac{L_m}{T_r} i_{qs}^{s} + \omega_r \psi_{dr}^{s} - \frac{1}{T_r}\psi_{qr}^{s} \quad (14)$$

Where, $T_r = \frac{L_r}{R_r}$

The rotor angle is estimated as follows:

$$\theta_e = \tan^{-1}\left(\frac{\psi_{qr}^{s}}{\psi_{dr}^{s}}\right) \quad (15)$$

Hence, speeds of the rotor is computed by using following equations,

$$\omega_r = \frac{d}{dt}\theta_e = \frac{1}{\psi_r^2}\left[\left(\psi_{dr}^{s}\frac{d}{dt}\psi_{qr}^{s} - \psi_{qr}^{s}\frac{d}{dt}\psi_{dr}^{s}\right) - \frac{L_m}{T_r}\left(\psi_{dr}^{s} i_{qs}^{s} - \psi_{qr}^{s} i_{ds}^{s}\right)\right] \quad (16)$$

The integration of SVPWM with an induction motor significantly enhances performance and efficiency of system. Additionally, SVPWM helps in reducing THD, further contributing to system's overall stability and performance. Thus, the combination of SVPWM and induction motors proves to be a highly effective resolution for optimizing induction motor control in RES and other power-driven applications.

4 RESULTS AND DISCUSSION

In this paper, a boost converter for a PV grid-connected system with an ANN based MPPT controller is presented. To assess RES based system's performance, MATLAB simulations are performed. These findings support the adoption of this advanced control strategy for grid and BLDC Motor integrated PV systems. The parameters for PV system and Boost converter are provided in Table 1.

Table 1: The parameters for PV system and Boost converter

Parameters	Rating
PV system	
Open Circuit Voltage	37.25 *V*
Short Circuit Current	8.95 *A*
Series Connected Solar PV cell	2
Parallel Connected Solar PV cell	14
Maximum Power voltage	29.95 *V*
Maximum Current	8.35 *A*
Boost converter	
L	*1 mH*
C	*2200 µF*

Case 1: Constant Temperature and Irradiance

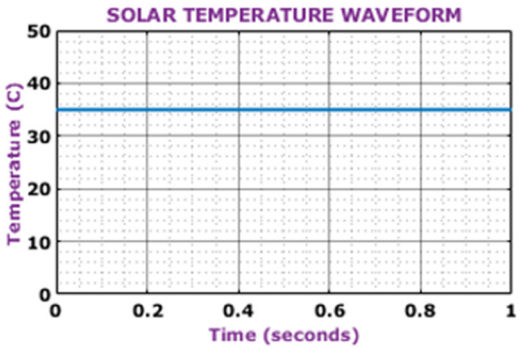

(a)

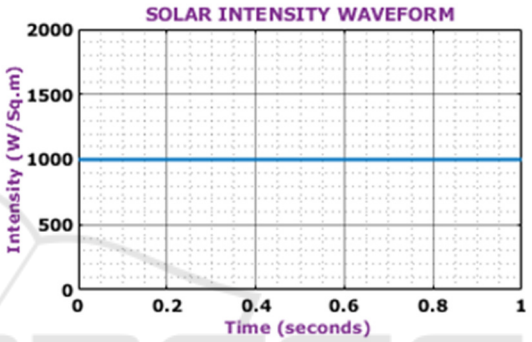

(b)

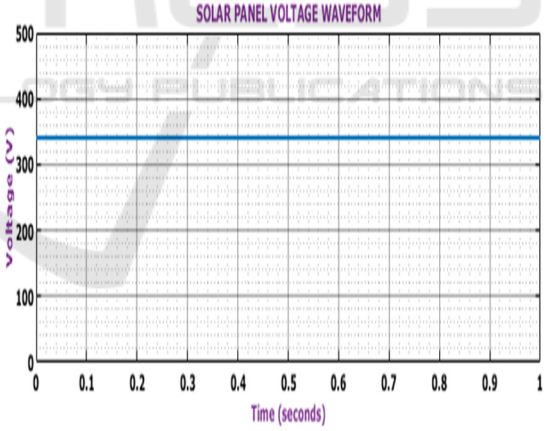

(c)

Figure 8: Solar panel (a) Temperature, (b) irradiance and (c) Voltage waveform

As shown in figure 8(a), temperature maintains continual at 35°C. Similarly, figure 8(b) illustrates that the irradiance remains steady at 1000 W/m², while figure 8(c) shows the voltage waveform maintaining a constant 340V.

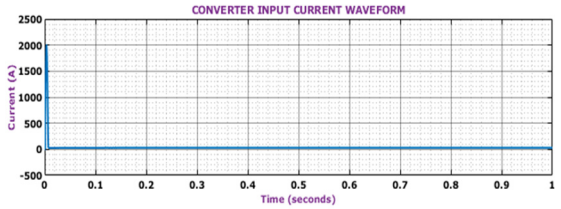

Figure 9: Converter input current waveform

The waveform of converter's input current peaks at 10A at 0.1 seconds, presenting a significant current flow at this time.

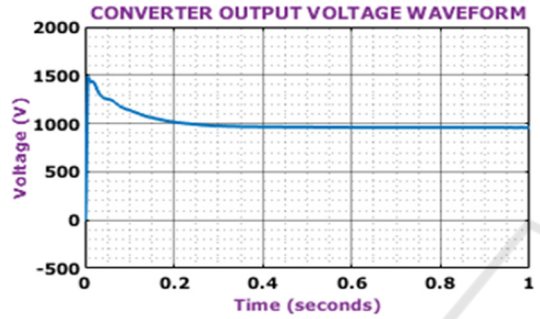

(a)

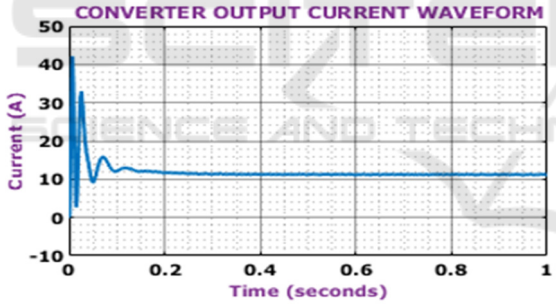

(b)

Figure 10: Converter output voltage and output current waveform

The waveforms in Figure 10 illustrate converter's output. The converter, aided by ANN based MPPT controller, consistently produces a stable voltage and current. The output voltage quickly stabilizes at 1000V within just 0.1s, while the current settles at 12A within the same brief period.

Figure 11 presents the power waveforms. In Figure 11(a), the input power waveform stabilizes at 10000 Watts following some initial fluctuations. Meanwhile, Figure 11(b) depicts the output power waveform, which reaches a peak within 0.1 seconds, before settling at a steady 12000 Watts for a duration of 0.05 seconds.

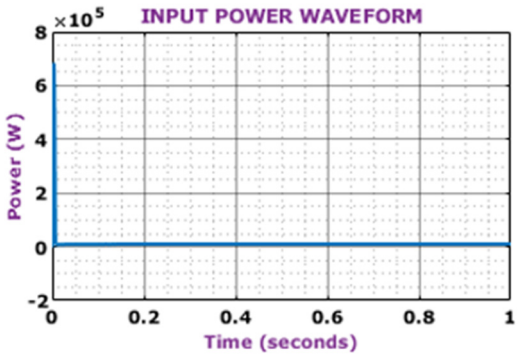

(a)

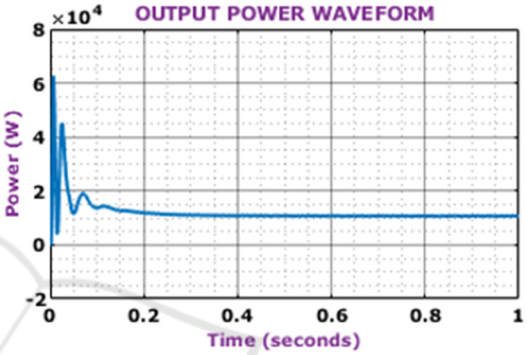

(b)

Figure 11: Power Waveform (a) Input and (b) Output

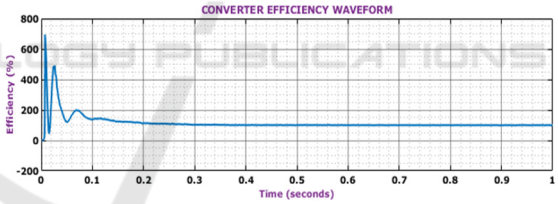

Figure 12: Waveform of Efficiency

The efficiency waveform in Figure 12 shows a rapid increase within the first 0.1 seconds, followed by stabilization around 83.3% for the remainder of the duration. This indicates a consistent and efficient performance of the system.

Case 2: Varying temperature and intensity

Figure 13 displays the solar panel's waveforms. A speedy and noticeable increase is seen in Figure 13(a), where temperature begins at 25°C and climbs to 45°C in 0.3 seconds. Figure 13(b) illustrates the irradiance waveform, which begins at 800 W/m² and increases to 1000 W/m² after 0.5 seconds. Finally, Figure 13(c) depicts the voltage waveform, which stabilizes at 340V.

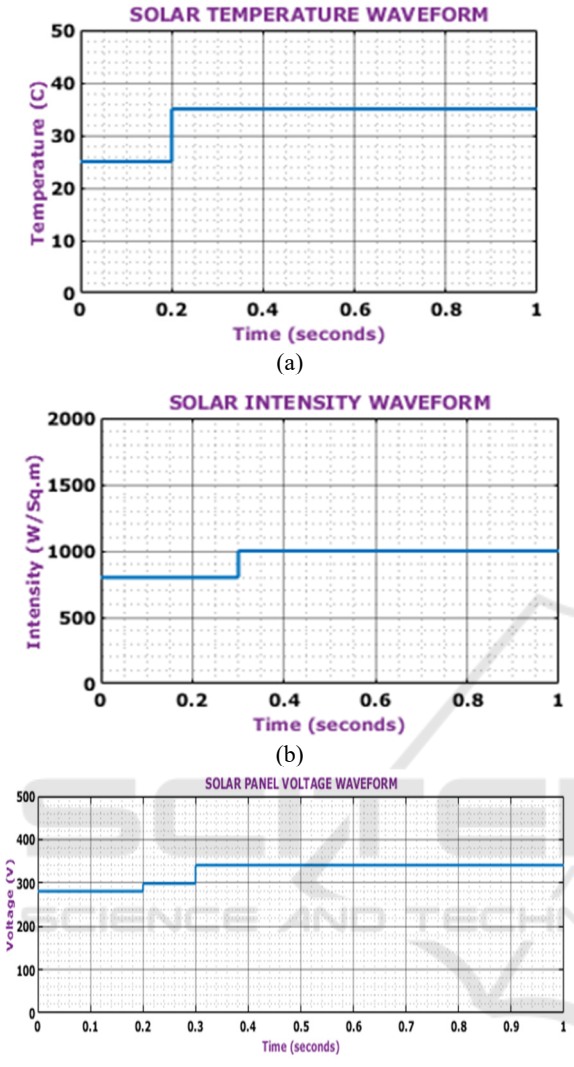

Figure 13: Solar panel waveform (a) Temperature, (b) Irradiance and (c) Voltage waveform under varying condition

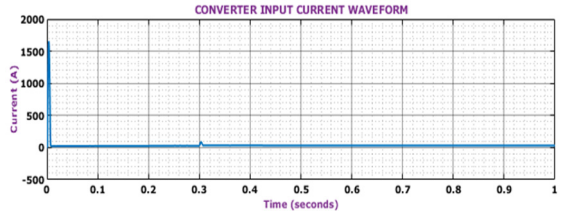

Figure 14: Converter input current waveform

The input current waveform of the converter reaches a peak of 10A at 0.1 seconds, indicating a substantial current flow at this moment.

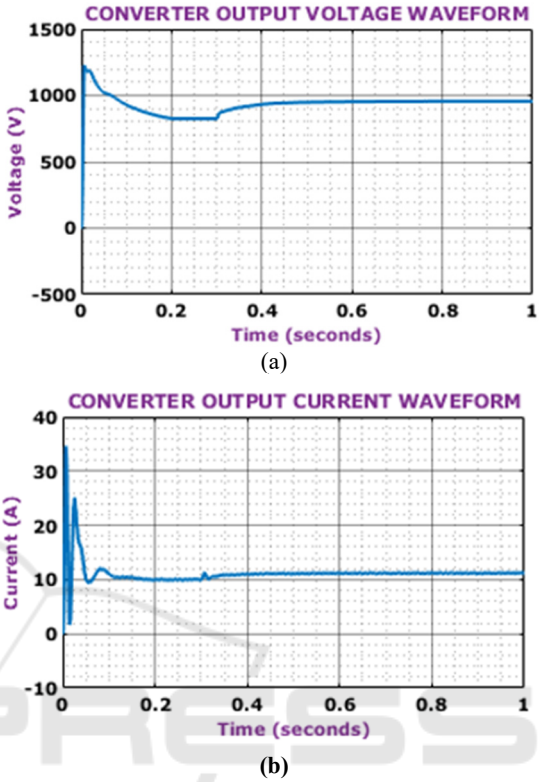

Figure 15: Converter output voltage and current waveform

The converter's output waveforms are displayed in Figure 15. The converter keeps the voltage and current steady with the help of ANN based MPPT controller. The output voltage quickly reaches 900V in 0.1 seconds, and the current reaches 11A in the same amount of time.

Figure 16 shows power waveforms: Figure 16(a) illustrates the input power stabilizing at 9000 Watts, while Figure 16(b) shows the output power peaking and settling at 110 Watts. Figure 16 (c) displays efficiency, rising quickly to stabilize at 81.8%.

Figure 17 illustrates the voltage waveforms of VAB, VBC, and VCA, each maintaining a consistent voltage level of 1200V over a duration of 1 second. These waveforms represent the balanced three-phase voltage outputs in the system which indicates a stable operation.

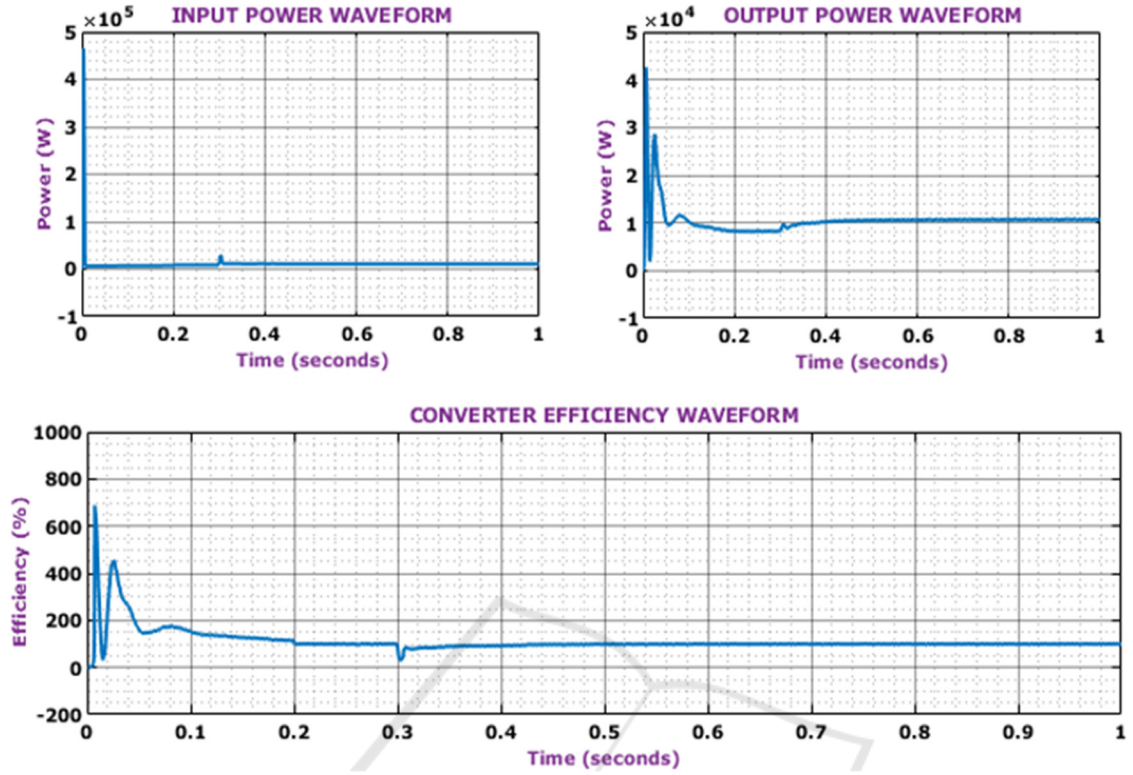

Figure 16: Waveform (a) Input Power, (b) Output Power and (c) Converter Efficiency

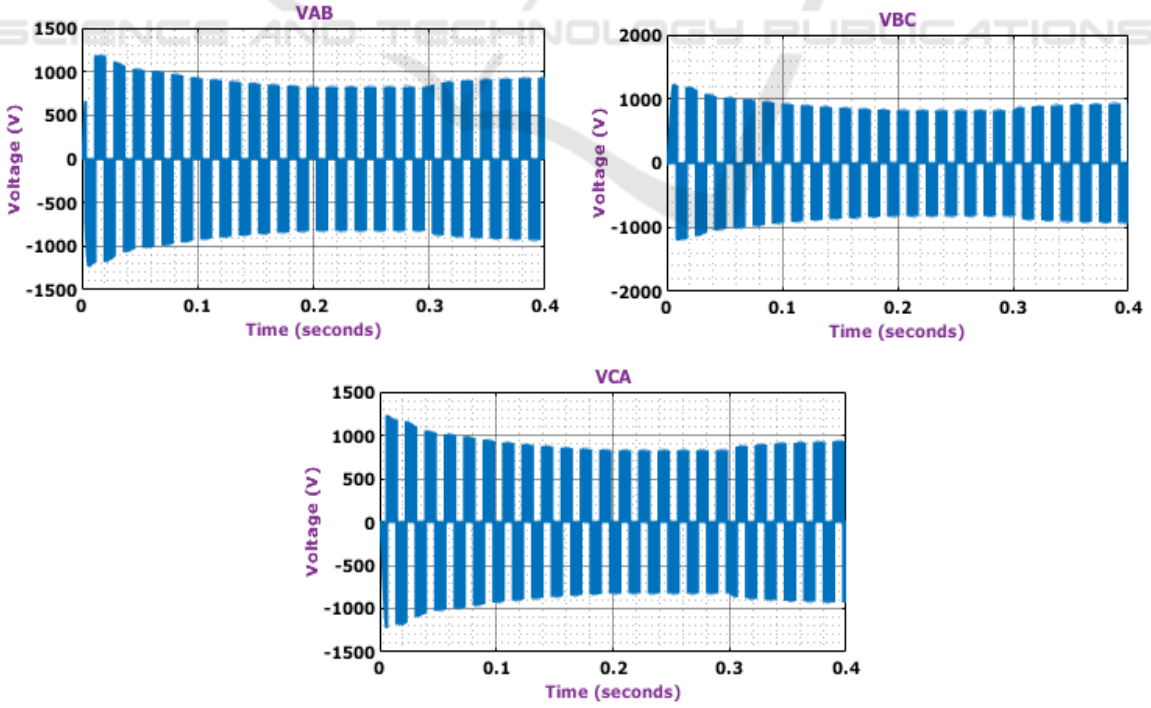

Figure 17: Voltage waveform (a) VAB, (b) VBC and (c) VCA

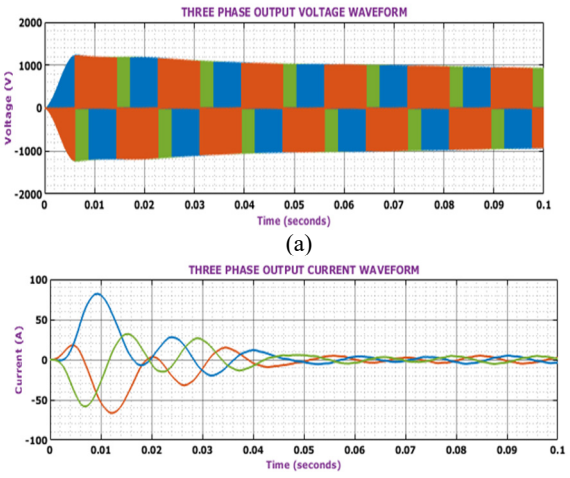

Figure 18: Three phase output waveform (a) Voltage, (b) Current

The three phase voltage waveform depicted in Figure 18(a) initially rises at a level of 1100V then falls down and in Figure 18 (b) represents the initial current value of 80A and then reduces gradually.

The Figure 19 (a) displays two waveforms of a BLDC motor. The graph shows the motor speed, initially rising rapidly to around 1800 RPM before stabilizing. The Figure 19 (b) illustrates the torque, which exhibits a sharp drop followed by a steady low value.

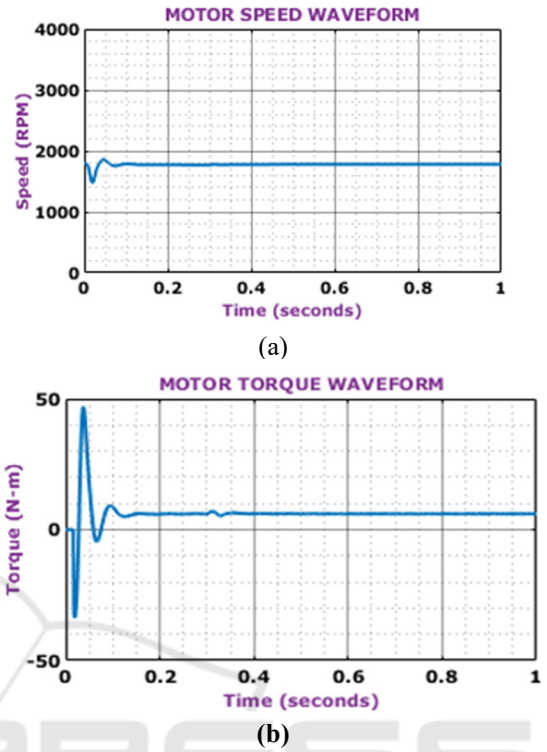

Figure 19: Waveform of BLDC (a) Speed, (b) Torque

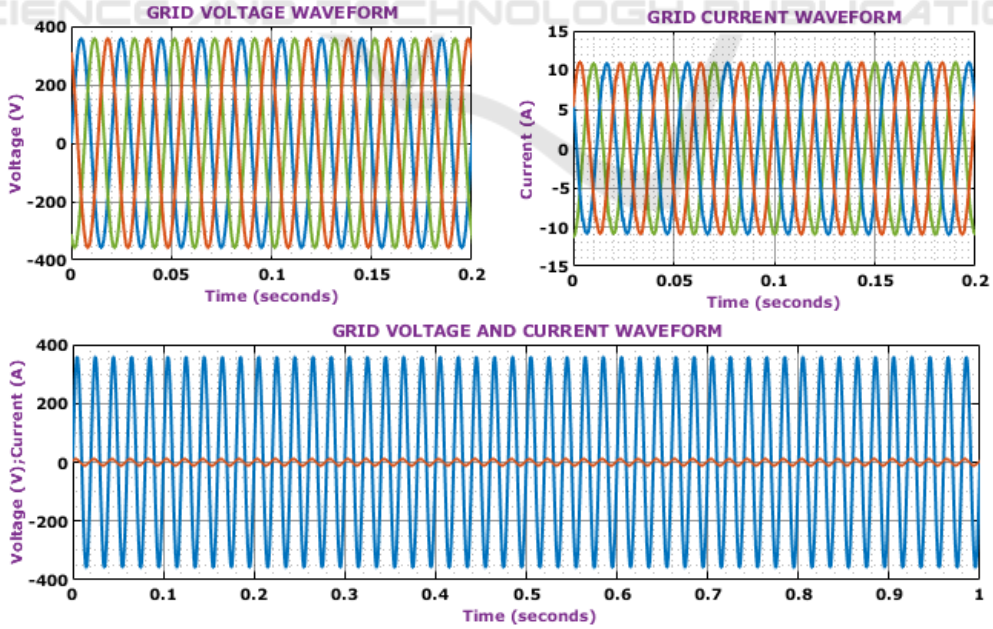

Figure 20: Grid Waveform (a) Voltage, (b) Current and (c) voltage and current

Figure 20 demonstrates grid voltage and current waveforms, highlighting effective grid voltage synchronization provided by the PI controller. Both waveforms are perfectly sinusoidal, in phase, with DFIG voltage at 370V and current at 12A. Figure 20(c) shows the pitch angle waveform of the DFIG.

Figure 21 illustrates the waveforms of real and reactive power. The reactive power gradually increases before stabilizing at a constant level (Fig. 21a), while the real power remains steady after a certain point (Fig. 21b).

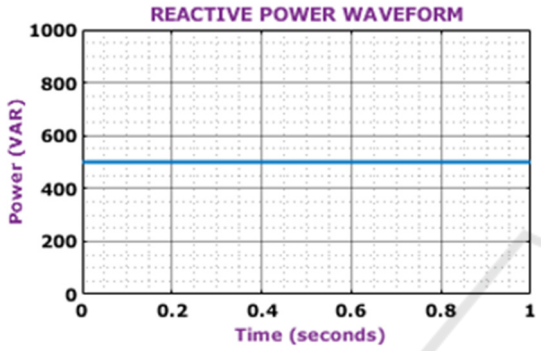

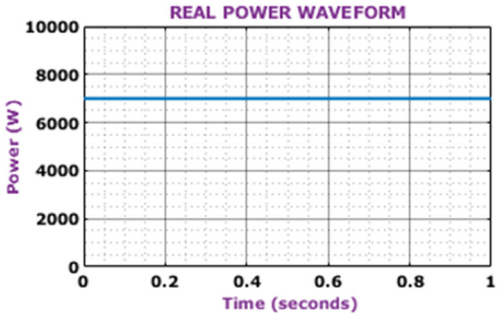

Figure 21: (a) Real power, (b) Reactive power waveform

Figure 22: illustrates Total Harmonic Distortion (THD) under three-phase grid conditions. As shown in 22(a), 22(b), and 22 (c), the harmonic distortion levels are 2.66%, 2.93%, and 2.03% for the R, Y, and B phases, respectively.

Table 2 Comparison of THD

Sl. No	References	THD
1	[16]	13%
2	[17]	6.1%
3	Proposed	2.03%

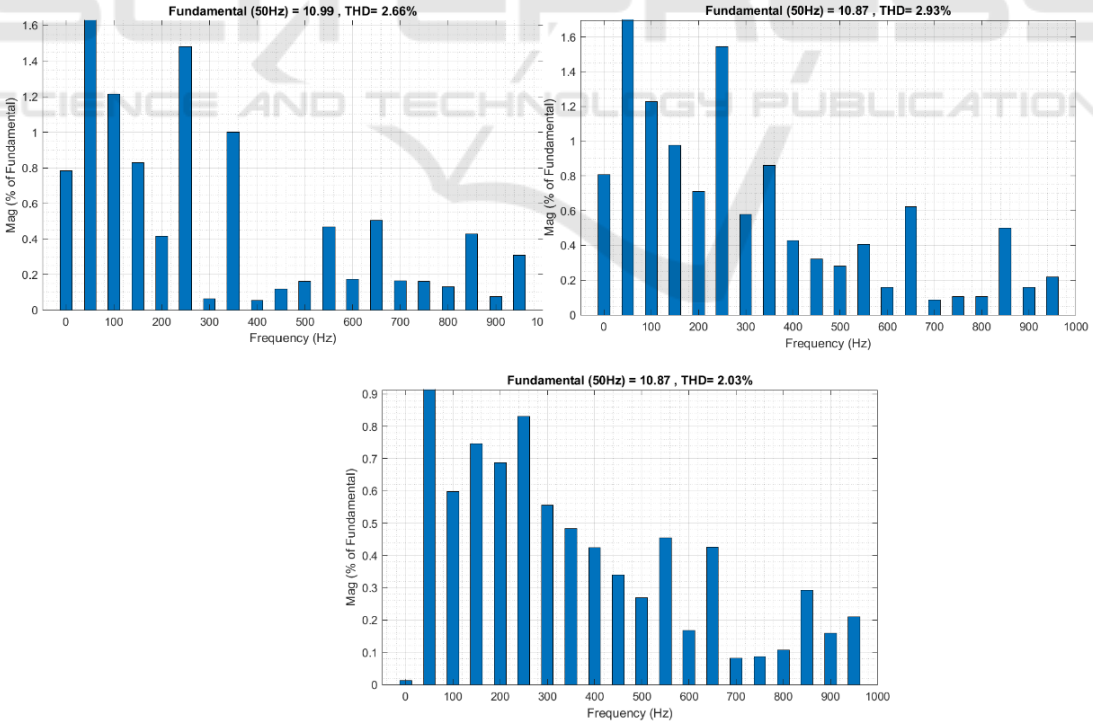

Figure 22: Total Harmonic Distortion (THD)

Table 2 presents a comparison of THD values, showing that the MPPT approach results in a minimized THD of 2.03%.

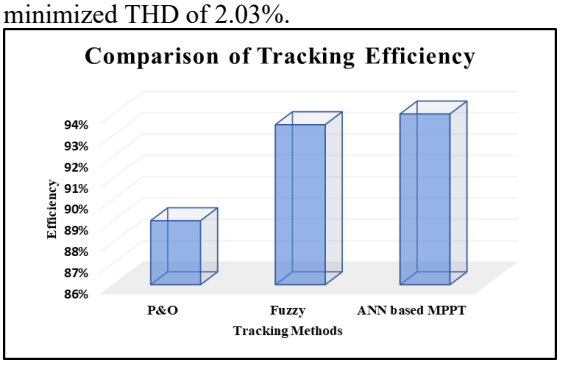

Figure 23: Comparison of Tracking Efficiency

The MPPT Tracking Efficiency Comparison of the values is shown in Figure 23, with the intended values for Perturbation & Observation (P&O) (Ali, Mousa, et al. 2023), Fuzzy (Kumar and Channi, 2022) and proposed ANN based MPPT being 88%, 93% and 93.5%, respectively.

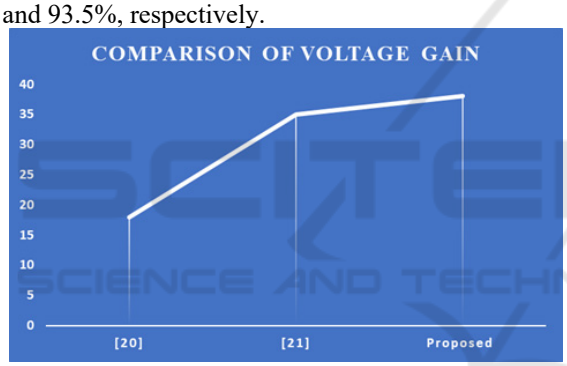

Figure 24: Comparison of Voltage Gain

Figure 24 illustrates the voltage gain of boost converters, with recorded values of 18, 35 and 38. In the proposed work, the converter achieves a voltage gain of 38.

5 CONCLUSION

In this paper, integration of a PV system with an induction motor and grid provides a promising solution for sustainable energy generation and efficient utilization in industrial and commercial applications. By constantly adapting to environmental changes like temperature and solar irradiation, an ANN based MPPT controller greatly increases efficiency of power extraction from the PV system. With better tracking precision and quicker convergence to the MPP, this unique MPPT method performs better than conventional algorithms. The efficient operation of the induction motor, driven by solar energy, minimizes energy losses, while the grid connection ensures stable power delivery and system balance. MATLAB simulation results show that proposed approach is effective, with a tracking efficiency of 93.5% and a THD value of 2.03%. Overall, this system represents a significant step forward in optimizing renewable energy utilization for sustainable power generation and efficient motor operation. Future advancements may focus on real-time implementation, Improved ANN technique, and improved grid integration to achieve greater efficiency, scalability, and reliability.

REFERENCES

Nahin, N. I., Biswas, S. P., Mondal, S., Islam, M. R., & Muyeen, S. M. (2023) A modified PWM strategy with an improved ANN based MPPT algorithm for solar PV fed NPC inverter driven induction motor drives. IEEE Access.

Villegas-Mier, C. G., Rodriguez-Resendiz, J., Álvarez-Alvarado, J. M., Rodriguez-Resendiz, H., Herrera-Navarro, A. M., & Rodríguez-Abreo, O. (2021) Artificial neural networks in MPPT algorithms for optimization of photovoltaic power systems: A review. Micromachines, 12(10): 1260.

Idrissi, Y. E. A., Assalaou, K., Elmahni, L., & Aitiaz, E. (2022) New improved MPPT based on artificial neural network and PI controller for photovoltaic applications. International Journal of Power Electronics and Drive Systems, 13(3): 1791-1801.

Harndi, H., Regaya, C. B., & Zaafouri, A. (2020) A sliding-neural network control of induction-motor-pump supplied by photovoltaic generator. protection and control of modern power systems, 5(1): 1-17.

Wongsathan, R. (2024) Integrated neural network-based MPPT and ant colony optimization-tuned PI bidirectional charger-controller for PV-powered motor-pump system. Engineering and Applied Science Research, 51(5): 605-617.

Yap, K. Y., Sarimuthu, C. R., & Lim, J. M. Y. (2020) Artificial intelligence based MPPT techniques for solar power system. Journal of Modern Power Systems and Clean Energy, 8(6): 1043-1059.

Chojaa, H., Derouich, A., Chehaidia, S. E., Zamzoum, O., Taoussi, M., & Elouatouat, H. (2021) Integral sliding mode control for DFIG based WECS with MPPT based on artificial neural network under a real wind profile. Energy Reports, 7: 4809-4824.

Elnozahy, A., Yousef, A.M., Abo-Elyousr, F.K., Mohamed, M. & Abdelwahab, S.A.M. (2021) Performance improvement of hybrid renewable energy sources connected to the grid using artificial neural network and sliding mode control. Journal of Power Electronics, 21: 1166-1179.

Bana, P. R., D'Arco, S., & Amin, M. (2024) ANN-based Robust Current Controller for Single-stage Grid-Connected PV with Embedded Improved MPPT Scheme. IEEE Access.

Vani, E., Balakrishnan, P., Singaram, G., & Senthil Kumar, S. (2024) PV Wind Battery Based Dc Microgrid with Neural Network MPPT. Journal of Electrical Systems, 20(5s): 430-437.

Al-Jaboury, O. N. R., Hamodat, Z., & Daoud, R. W. (2024) Design of Power Control Circuit for Grid-Connected PV System-Based Neural Network. Journal of Robotics and Control (JRC), 5(3): 821-828.

Mol, E. J., & Linda, M. M. (2023) Integration of wind and PV systems using genetic-assisted artificial neural network. Intelligent Automation and Soft Computing, 35(2): 1471-1489.

Gowid, S., & Massoud, A. (2020) A robust experimental-based artificial neural network approach for photovoltaic maximum power point identification considering electrical, thermal and meteorological impact. Alexandria Engineering Journal, 59(5): 3699-3707.

Kiran, S. R., Basha, C. H., Singh, V. P., Dhanamjayulu, C., Prusty, B. R., & Khan, B. (2022) Reduced simulative performance analysis of variable step size ANN based MPPT techniques for partially shaded solar PV systems. IEEE access, 10: 48875-48889.

Mohammad, K. A. (2024) Optimization Of Solar Energy Efficiency Using Neural Network Controllers With Direct Current Converters.

Kumar, P. S., Sridhar, S., & Kumar, T. R. (2014) Design & simulation of boost converter for power factor correction and THD reduction. Int. Jr. of ScientificEngg. & Tech. Res. IJSETR, 3(42): 8462-8466.

Nazarkar, S., & Shelar, S. (2016) Design & Simulation Of Active Power Factor Controller Using Boost Converter. International Journal of Innovations in Engineering Research and Technology, 3(3): 1-8.

Ali, A. I. M., Mousa, H. H., Mohamed, H. R. A., Kamel, S., Hassan, A. S., Alaas, Z. M., ... & Abdallah, A. R. Y. (2023) An Enhanced P&O Mppt Algorithm With Concise Search Area For Grid-Tied Pv Systems. IEEE Access, 11: 79408-79421.

Kumar, R., & Channi, H. K. (2022) A PV-Biomass off-grid hybrid renewable energy system (HRES) for rural electrification: Design, optimization and techno-economic-environmental analysis. Journal of Cleaner Production, 349: 131347.

Pirpoor, S., Rahimpour, S., Andi, M., Kanagaraj, N., Pirouzi, S., & Mohammed, A. H. (2022) A novel and high-gain switched-capacitor and switched-inductor-based DC/DC boost converter with low input current ripple and mitigated voltage stresses. IEEE Access, 10: 32782-32802.

Ahmad, J., Zaid, M., Sarwar, A., Lin, C. H., Asim, M., Yadav, R. K., ... & Alamri, B. (2021) A new high-gain dc-dc converter with continuous input current for dc microgrid applications. Energies, 14(9): 2629.